

Galilean Invariant Extraction and Iconic Representation of Vortex Core Lines

J. Sahner, T. Weinkauff, H.-C. Hege

Zuse Institute Berlin (ZIB), Berlin, Germany — {sahner, weinkauff, hege}@zib.de

Abstract

While vortex region quantities are Galilean invariant, most methods for extracting vortex cores depend on the frame of reference. We present an approach to extracting vortex core lines independently of the frame of reference by extracting ridge and valley lines of Galilean invariant vortex region quantities. We discuss a generalization of this concept leading to higher dimensional features. For the visualization of extracted line features we use an iconic representation indicating their scale and extent. We apply our approach to datasets from numerical simulations and experimental measurements.

Categories and Subject Descriptors (according to ACM CCS): I.3.3 [Computer Graphics]: Line and Curve Generation I.3.3 [Computer Graphics]: Picture/Image Generation I.3.7 [Computer Graphics]: Three-Dimensional Graphics and Realism

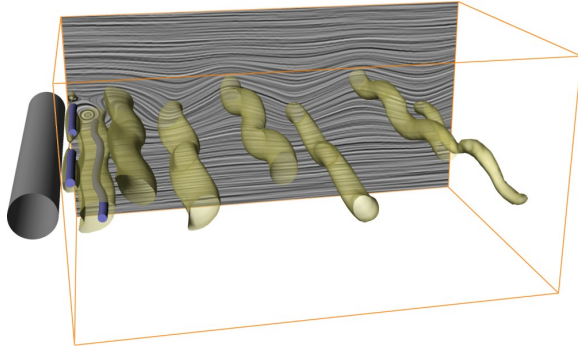
1. Introduction

Flow fields play a vital role in many research areas. Examples are burning chambers, turbomachinery and aircraft design in industry as well as visualization and control of blood flow in medicine. As the resolution of numerical simulations as well as experimental measurements like PIV have evolved significantly in the last years, the challenge of understanding the intricate flow structures within their massive result data sets has made automatic feature extraction schemes popular.

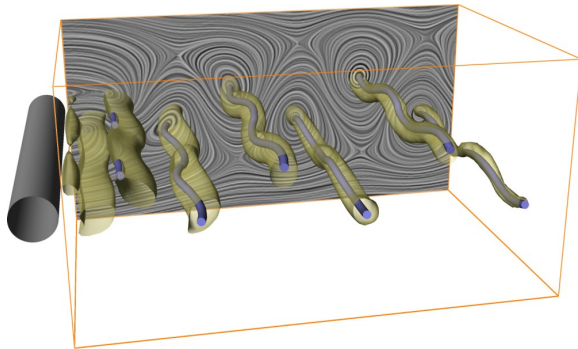
Among the features of interest are topological and vortical structures. Topological visualization methods have been introduced to the visualization community in [HH89] and have been extended since then [GLL91, SKMR98, dLvL99, WS01, TWHS03, WTHS04]. While they aim at the segmentation of a vector field into areas of different flow behavior, vortex oriented methods highlight turbulent regions of the flow. Recently some work has been done to link these different areas: [GTS04, TKG*04] employ topological methods to analyze the phenomenon of vortex breakdown. Vortices play a major role due to their wanted or unwanted effects on the flow. In turbomachinery design, vortices reduce efficiency, whereas in burning chambers, vortices have to be controlled to achieve optimal mixing of oxygen and fuel. In aircraft design, vortices can both increase and decrease lift. While

[PVH*02] and [PR99] give a thorough overview of algorithms for the treatment of vortical structures, we give a short introduction here. They can be classified in two major categories:

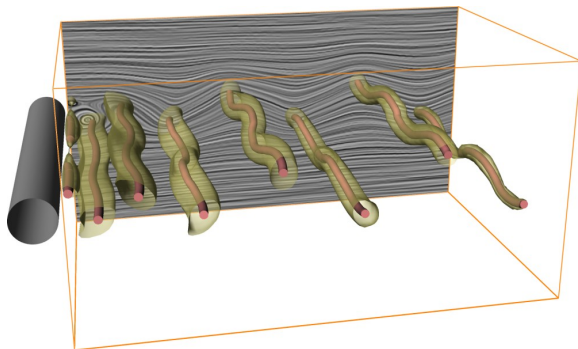
- *Vortex region detection* is based on scalar quantities that are used to define a vortex as a spatial region where the quantity exhibits a certain value range. We refer to them as *vortex region quantities*. Examples of this are regions of high magnitude of vorticity or negative λ_2 -criterion [JH95] (cf. Figure 1). In general, these measures are Galilean invariant, i.e., they are invariant under adding constant vector fields. This is due to the fact that their computation involves derivatives of the vector field only. Isosurfaces or volume rendering are common approaches for visualizing these quantities, which requires the choice of thresholds and appropriate isovalues or transfer functions. As shown in [RP96], this can become a difficult task for some settings.
- *Vortex core line extraction* aims at extracting line type features that are regarded as centers of vortices. Different approaches exist. [SH95, PR99] consider lines where the flow exhibits a swirling motion around it. [BS95] extracts vorticity lines seeded at critical points and corrected towards pressure minima. [RP98] considers stream lines of zero torsion. All of these approaches include a Galilean



(a) Original frame of reference. Vortex core lines following the approach of [SH95, PR99].



(b) Alternative frame of reference. Vortex core lines following the approach of [SH95, PR99].



(c) Our Galilean invariant approach. Vortex core lines extracted as valley lines of λ_2 .

Figure 1: Flow behind a circular cylinder. Vortex regions visualized as transparent isosurfaces of λ_2 . Vortex core lines displayed as cylindrical lines.

variant part, i.e., they depend on a certain frame of reference (Figures 1a-b). In contrast to vortex region detection described above, the extraction of those lines is parameter free in the sense that their definition does not refer to a range of values. This eliminates the need of choosing certain thresholds.

In this paper we present an approach to extracting vortex core lines that is invariant under Galilean changes of the reference frame. I.e., the extracted features remain unchanged when a constant vector is added to the flow field. Instead of using swirling stream line behavior as indication of a vortex core line, we consider ridge or valley lines of Galilean invariant vortex region quantities (Figure 1c). Furthermore, we show that those line type features have a higher dimensional generalization, e.g., surfaces.

The article is organized as follows: sections 2.1 and 2.2 review the most important approaches to vortex region detection and vortex core line extraction. While section 2.3 treats the theory of ridge and valley lines, section 3 deals with implementation issue for their extraction. In Section 4 we present an iconic representation for vortex core lines that encodes the most relevant information like strength of the coherent structure as well as rotation direction. We apply our technique to several data sets in section 5.

2. Theoretical Background

We now give a short introduction to the two vortex detection approaches mentioned above and suggest a combination of both in subsection 2.3.

2.1. Vortex Region Detection

There are several derived scalar quantities that indicate vortex activities. Ranging from simple to involved, vortices might be defined as regions of high magnitude of vorticity $\omega = (\omega_1, \omega_2, \omega_3)^t = \nabla \times v$, low pressure p , rotation strength Δ , positive Q -criterion and negative λ_2 -criterion. In the following, we give some details on the three latter quantities.

Rotation strength Δ as used in [SP03], see also [CPC90] is linked to the intuitive understanding that a vortex exhibits spiraling stream lines with respect to some specific reference frame. Within this reference frame, the stream line pattern of a flow field is dominated by its Jacobian Jv . If J has a conjugate pair of complex eigenvalues, the flow locally spirals in a plane corresponding to those eigenvectors. Δ is then defined as the magnitude of the imaginary part of those complex conjugate eigenvalues. So large values of Δ indicate strong spiraling patterns within the right reference frame. Where $\Delta = 0$, no such reference frame can be found. By considering the orientation of the corresponding eigenbasis, a rotation angle $\varphi \in (-\pi, \pi)$ can also be extracted. When $\varphi > 0$, the flow spirals counter clockwise around the eigenvector corresponding to the real eigenvalue, clockwise, if $\varphi < 0$.

The closely linked quantities Q and λ_2 are related to the Navier Stokes equations and reflect the amount of strain and vortical motions in the vector field. Due to this fact those quantities are the most popular among fluid mechanicians. Let ∇v denote the gradient of the vector field. Then the strain tensor \mathbf{S} is defined as its symmetric part $\mathbf{S} = \frac{1}{2}(\nabla v + \nabla v^t)$.

The antisymmetric part $\Omega = \frac{1}{2}(\nabla v - \nabla v^t)$ is closely related to vorticity obeying

$$\Omega = \begin{pmatrix} 0 & -\omega_3 & \omega_2 \\ \omega_3 & 0 & -\omega_1 \\ -\omega_2 & \omega_1 & 0 \end{pmatrix}.$$

Then the Q -criterion defined by [Hun87], also known as the Okubo-Weiss criterion, is defined by

$$Q := \frac{1}{2}(\|\Omega\|^2 - \|\mathbf{S}\|^2) = \|\omega\|^2 - \frac{1}{2}\|\mathbf{S}\|^2.$$

Q has a direct physical interpretation. Where $Q > 0$, vorticity dominates strain, so Hunt identified vortex regions with $Q > 0$. Note that $Q < 0$ indicates that the vector field is dominated by strain, making this criterion valuable in vector fields with distinct areas of strong vortical motions and areas of high strain.

λ_2 , derived by [JH95], is closely related to Q . Consider the three real eigenvalues $\lambda_1 \leq \lambda_2 \leq \lambda_3$ of the symmetric matrix $\mathbf{S}^2 + \Omega^2$. In [JH95] it is deduced from the Navier Stokes equations that for a local pressure minimum two negative eigenvalues of this matrix are necessary. They define a vortex region where $\lambda_2 < 0$. In their work they show that $Q = -\frac{1}{2}(\lambda_1 + \lambda_2 + \lambda_3)$. Despite of this strong link they show that the λ_2 -criterion detects vortex regions more reliably especially under a strong external strain. Nevertheless, the λ_2 -criterion, unlike the Q -criterion, lacks a direct interpretation for regions where $\lambda_2 > 0$.

The Q -criterion is very fast to compute. Where the λ_2 criterion involves computation of eigenvalues of a (symmetric) matrix, Q can be computed quickly using the identity $Q = -\sum_{i,j}(\nabla v)_{ij}(\nabla v)_{ji}$.

Despite the convincing physical interpretation, those quantities are of limited applicability in some settings. In [RP96] it is shown that for turbomachinery flow fields λ_2 is negative almost everywhere. So for highlighting regions of strong vortical activity thresholding is necessary, leaving the scientist with the question of choosing an appropriate iso-value. So vortex region detection has the drawback of being parameter dependent.

2.2. Vortex Core Line Extraction

Several algorithms aim at extracting a line feature called the vortex core line. The motivation arises from the intuitive observation that a vortex might be regarded as circular particle movement around a common line.

It was suggested in [MK97] to consider minimal lines of pressure. This approach was applied locally only and resulted in disconnected line segments. In contrast to this, our method results in continuous lines. Furthermore, we consider arbitrary vortex region quantities. In [SH95] a technique was developed where vortex core lines are identified with locations where the velocity points into the direction of

the eigenvector of the real eigenvalue of ∇v in places where it has two complex eigenvalues indicating a vortical movement around the real eigenvector (and thus around the vector field). This technique was improved in [PR99], where the parallel vectors approach ensured connected lines. The same authors suggested in [RP98] a higher order method for vortex core line extraction of lines with zero torsion, which also involves the vector field v directly by finding line structures where v points into the direction of $(\nabla a)v$ where $a = (\nabla v)v$ is the acceleration of the vector field. Another prominent approach is due to [BS95]. Here vorticity is integrated starting from critical points in the vector field and corrected towards pressure minimum.

The last three approaches have the drawback of being dependent on the reference frame. Choosing the right reference frame for the approaches of [SH95, RP98] may result in a vortex core line, but when the spectator changes the reference frame significantly (for instance by moving faster than the mean velocity of the field), the feature vanishes. Figure 1 shows this dependence on the reference frame. In [BS95] the extraction of critical points is Galilean variant.

The advantage of those schemes over the vortex region approach is that they can be applied without user interaction, for instance as a batch job prior to visualization or during the simulation.

2.3. Ridge and Valley Lines for vortex core line extraction

We suggest a combination of both approaches by extracting vortex core lines of vortex region quantities like Q and λ_2 and identify those lines by certain maximal lines of Q called ridge lines where $Q > 0$ and certain minimal lines of λ_2 where $\lambda_2 < 0$ called valley lines. In [PR99] it is pointed out how to extract such extremum lines using the parallel vectors operator. We use the Feature Flow Field approach due to [TS03] detailed in section 3.

By extracting vortex core lines in this way, we combine the Galilean invariance of the vortex region detection with the parameter independence of the vortex core line extraction.

Several notions of extremum lines, ridge and valley lines of a function $f : \mathbf{R}^3 \rightarrow \mathbf{R}$ have been developed in the literature. We use the height ridge definition detailed in [Ebe96], which is a one dimensional generalization of the well known zero dimensional notion of an extremum point. We choose this definition as it requires just second derivatives of the vector field rather than fourth order derivatives like ridge definitions that are based on curvature extrema, see [EGM*94] for a thorough introduction and comparison of several ridge line extraction schemes and [KvD93] for a historical survey of the development of extremum lines.

A sufficient condition for a local maximum point x of a

function $f : \mathbf{R}^3 \rightarrow \mathbf{R} \in C^2(\mathbf{R}^3; \mathbf{R})$ is a vanishing gradient $\nabla f(x) = 0$ coupled with a negative definite Hessian $Hf(x)$ implying a set of three negative eigenvalues $\gamma_1 \leq \gamma_2 \leq \gamma_3$ corresponding to orthogonal eigenvectors $c_1, c_2, c_3 \in \mathbf{R}^3$ satisfying $Hc_i = \gamma_i c_i$. As H is symmetric, such an orthogonal eigensystem corresponding to real eigenvalues always exists.

Aiming at a one dimensional generalization of a local maximum, we note that negative eigenvalues γ_i imply that the graph of f is convex in a small neighbourhood of the maximum. In direction of c_3 , the eigenvector corresponding to the largest eigenvalue γ_3 , the maximum is least stable, as this is the direction of smallest convexity. The softest relaxation hence is to relax convexity just in direction of c_3 . As a ridge line (when looking at a terrain) should intuitively follow the steepest ascend, it is natural to require $c_3 = \mathbf{const} \cdot \nabla f$ whenever $\nabla f \neq 0$, resulting in the requirement $H(\nabla f) = \gamma_3(\nabla f)$. This makes ridge line extraction applicable to the parallel vectors operator as stated in [PR99]. From the orthogonality of c_i , it directly follows that $(\nabla f)c_1 = 0, (\nabla f)c_2 = 0$. Vice versa, $(\nabla f)c_1 = (\nabla f)c_2 = 0, \nabla f \neq 0$ implies that $c_3 = \mathbf{const} \cdot \nabla f$, also from orthogonality.

This intuition leads to the following definition cited from [Ebe96].

Definition 1 Let $f \in C^2(\mathbf{R}^3; \mathbf{R})$, ∇f its gradient and Hf its Hessian with eigenvectors c_1, c_2, c_3 and corresponding eigenvalues $\gamma_1 \leq \gamma_2 \leq \gamma_3$.

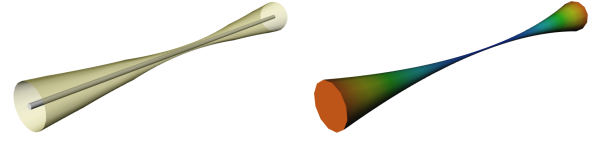
1. Then a ridge line consists of all points x where
 - $A := (\nabla f(x))c_1 = 0$ and $B := (\nabla f(x))c_2 = 0$ and
 - $\gamma_2 < 0$.
2. This has a d -dimensional generalization. A d -dimensional ridge consists of all points x where
 - $\nabla f(x)c_i = 0$ for all $i = 1, \dots, 3 - d$ and
 - $\gamma_{3-d} < 0$.
3. d -dimensional valleys of f are defined as d -dimensional ridges of $-f$.

Note that the structures defined here are d -dimensional manifolds in most cases due to the regular value theorem justifying the terminology of d -dimensional ridges.

As an example let $\gamma_1 \leq \gamma_2 < 0, \gamma_3 > \gamma_2$ and consider the function $f(x, y, z) = \gamma_1 x^2 + \gamma_2 y^2 + \gamma_3 z^2$. Then $\nabla f(x, y, z) = (\gamma_1 x, \gamma_2 y, \gamma_3 z)^t$, $Hx(x, y, z) = \text{diag}(\gamma_1, \gamma_2, \gamma_3)$ with eigenbasis $c_i = e_i, e_i$ denoting the euclidean standard basis. At $x = y = 0$ we have $\nabla f(x)a = \nabla f(x)b = 0$ and $\gamma_2 < 0$. Hence, the z -axis is a ridge line. Figure 2 illustrates this for $\gamma_1 = -100, \gamma_2 = -99, \gamma_3 = 1$.

With the notion of d -dimensional ridges at hand we can define d -dimensional **Galilean invariant vortex cores**.

Definition 2 Let s be a Galilean invariant vortex region quantity. In regions where s identifies a vortex, a d -dimensional



(a) Ridge line is in the center of the isosurface (transparent). (b) Ridge line scaled and colored according to the scalar value.

Figure 2: Ridge line of a simple scalar field.

vortex region quantity	vortex range	vortex core type
p	$[0, \infty)$	valley
$\ \omega\ $	$(0, \infty)$	ridge
Δ	$(0, \infty)$	ridge
Q	$(0, \infty)$	ridge
λ_2	$(-\infty, 0)$	valley

Table 1: Vortex region quantities pressure p , vorticity ω , rotation strength Δ from [SP03], Q -criterion and λ_2 criterion with the value range in which they indicate vortices. Vortex cores according to definition 2 are either ridges or valleys as shown in column 3.

Galilean invariant vortex core with respect to s is defined as d -dimensional

$$\left. \begin{array}{l} \text{ridge} \\ \text{valley} \end{array} \right\} \text{ of } s \text{ if } \left\{ \begin{array}{l} \text{large} \\ \text{small} \end{array} \right.$$

values of s indicate a vortex.

This paper is devoted to extracting 1-dimensional vortex cores that we suggest as an alternative definition of vortex core lines. Nevertheless, 2-dimensional vortex cores are interesting features for future research.

Several vortex region quantities s and their vortex indicating value ranges are displayed in Table 1. This table also shows, whether vortex cores with respect to s are ridges or valleys of s .

3. Extraction of Vortex Core Lines

Let s be a vortex region quantity as used in Definition 2. We use the Feature Flow Field extraction scheme from [TS03] to extract the vortex core lines with respect to s as defined in the previous subsection.

The Feature Flow Field scheme involves two steps: In the first step certain points are extracted that lie on the extremum lines of interest. Those points are used as seed points in the second step by extracing the extremum lines as field lines

of a derived flow field, the so called feature flow field. The following subsection is devoted to these two issues.

Afterwards we address interpolation issues in Subsection 3.2. The applications we show in Section 5 are based on flow fields that are interpolated from uniform grid data. We found that the widely used trilinear interpolation is not well suited for ridge extraction.

3.1. Feature Flow Field setup

Again, we concentrate on the extraction of ridge lines. From Definition 1 in the previous subsection, we know that we have to extract regions where $A = B = 0, \gamma_2 < 0$.

Assuming a point $x \in \mathbf{R}^3$ fulfills this requirement, the tangent direction of the ridge x lies on can be computed as follows. As ∇A is orthogonal to the isolines of A and ∇B is orthogonal to the isolines of B , the ridge tangent is $T := \nabla A \times \nabla B$. The ridge line passing through x is then exactly the field line of T passing through x . So T is the feature flow field we are looking for. We extracted the ridge lines by Runge-Kutta-integration of T . Although T involves derivatives of high degree, we still found that integrating the features was stable.

Now we are left with computing T and finding seed points x .

3.1.1. Finding seed points

We are searching for zeros of the mapping $x \mapsto (A, B)$ from $\mathbf{R}^3 \rightarrow \mathbf{R}^2$. As we expect the zeros to be one dimensional, we can restrict the search to two dimensional subsets of the domain, e.g., the faces of some underlying structured or unstructured grid. This reduces the problem to finding roots of a function $\mathbf{R}^2 \rightarrow \mathbf{R}^2$. For this setting, several Newton solvers can be applied, involving further differentiation. As $A = (\nabla f)c_1$ and $B = (\nabla f)c_2$ already involve second derivatives of f , we favoured a gradient free minimization of the positive function $x \mapsto A^2 + B^2$ which turned out to be more stable. We used the method described in [Ebe96] based on Powell's search [Pow64] and inverse parabolic interpolation [PFTV91].

3.1.2. Computing the feature flow field

The computation of the feature flow field $T := (\nabla A) \times (\nabla B)$ is quite involved. First of all, it is not trivial to state ∇A and ∇B explicitly in terms of the derivatives of f . Furthermore, A and B might be discontinuous at places where $\gamma_1 = \gamma_2$, so called partial umbilics. At such places the Eigensystem γ_i is not unique, because the 2-dimensional eigenspace corresponding to $\gamma_1 = \gamma_2$ allows a range of orthonormal bases. [Ebe96] provides a remedy for this issue. As those findings are central to our algorithm, we state the ridge direction computed therein. The ridge tangent T is given by

$$T = \tilde{A} \times \tilde{B}. \quad (1)$$

Here, $\tilde{A}, \tilde{B} \in \mathbf{R}^3$ are given by

$$\begin{Bmatrix} \tilde{A}_i \\ \tilde{B}_i \end{Bmatrix} = \begin{Bmatrix} \gamma_1 c_{1i} + \frac{(\nabla f)c_3}{\gamma_1 - \gamma_3} \sum_{j,k} c_{1j} \gamma_{3k} \partial_{x_i} \partial_{x_j} \partial_{x_k} f \\ \gamma_2 c_{2i} + \frac{(\nabla f)c_3}{\gamma_2 - \gamma_3} \sum_{j,k} c_{2j} c_{3k} \partial_{x_i} \partial_{x_j} \partial_{x_k} f \end{Bmatrix}. \quad (2)$$

In [Ebe96] it is shown that T is only defined up to sign, whenever the ridge passes a partial umbilic $\gamma_1 = \gamma_2$. So in practice, when following a ridge by integrating T , the current ridge direction t_1 is compared to the previous ridge direction t_0 and replaced by $-t_1$ if the euclidean scalar product $t_1 \cdot t_0 < 0$, i.e., if two subsequent ridge directions differ by an angle greater than $\frac{\pi}{2}$.

3.2. Interpolation issues

For ridge and valley line extraction, gradient and hessian of vortex region quantities s have to be computed at arbitrary locations. As s usually involve derivatives of the flow to be Galilean invariant, the hessian Hs involves third derivatives of the flow field. [PR99] states that extracting extremum lines requires careful filtering of the input field. We suggest here to use an appropriate interpolation scheme to remedy this problem.

Interpolating s trilinearly appeared to be both unstable and ineffective. Although some features were roughly recognized, most of them were missed completely. This is not surprising due to the high degree of smoothness required by the setting, and the fact that extremum lines are typically quadratic features that can not be resolved well by trilinear interpolation. Due to this, quadratic schemes seem a natural choice. Among those, approximation by quadratic super splines (see [RZNS04]) provides a good trade-off between smoothness and speed. As the polynomials involved are of total degree 2, (2) simplifies significantly, as here $\partial_{x_i} \partial_{x_j} \partial_{x_k} f = 0$ for all i, j, k and hence, (2) can be restated as follows:

$$\tilde{A}_{QSS} = \gamma_1 c_1, \quad \tilde{B}_{QSS} = \gamma_2 c_2, \quad (3)$$

and, if $\nabla f \neq 0$, the ridge tangent T from (1) evaluates to

$$T_{QSS} = \gamma_1 \gamma_2 c_1 \times c_2 = \mathbf{const} \cdot \nabla f, \quad (4)$$

conforming to the intuitive understanding of a ridge direction as stated in subsection 2.3. This makes quadratic super splines a somewhat natural choice.

4. Iconic Representation

To visualize vortex core lines, we use cylindrical meshes and encode different scalar values into their representation. Figure 3 illustrates this. In figures 3a-b we color or scale the cylinder according to the mapped values. Figures 3c-d encode sign and strength of a rotational behavior, either by using colored stripes on the cylinder itself or by placing a spiral shape around it. Our implementation allows us to combine these four variations as shown in figures 3e-f and 2b. Note, that not all possible combinations produce expressive

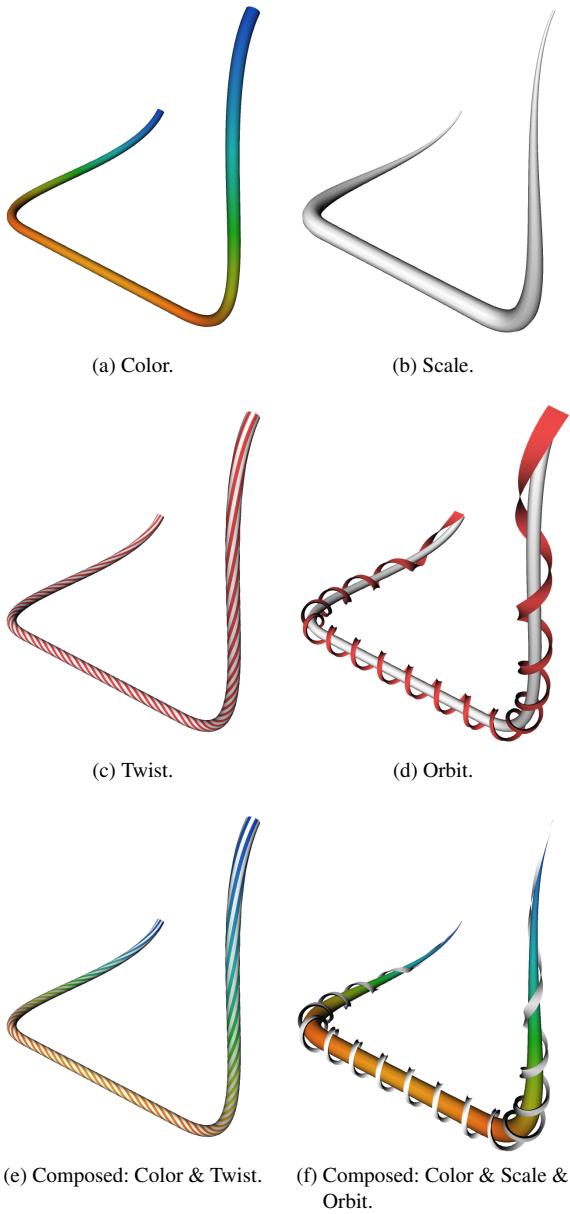


Figure 3: Different approaches to encoding a scalar value into the representation of a line.

results. Especially the usage of an orbit (figure 3d) tends to yield cluttered visualizations in more involved settings.

While those kinds of representing a line are quite common, we are still left with finding appropriate measures to be mapped onto our Galilean invariant vortex core lines. [JMT02] depicts spiraling stream lines around a Galilean variant vortex core line. As we treat Galilean invariant vortex core lines in this paper, this approach is not directly ap-

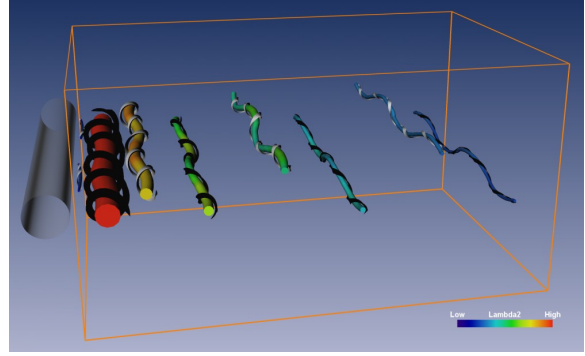


Figure 4: Flow behind a circular cylinder. Iconic representation of Galilean invariant vortex core lines. λ_2 was used for extraction and is encoded into color and scale of the cylindrical meshes. Red / blue color is used to indicate strong / weak vortex activity. φ is encoded into color and spiral direction of the orbits.

plicable. [SP03] extracts and displays vortex hulls similar to isosurfaces of Δ (see section 2.1) around a vortex core line.

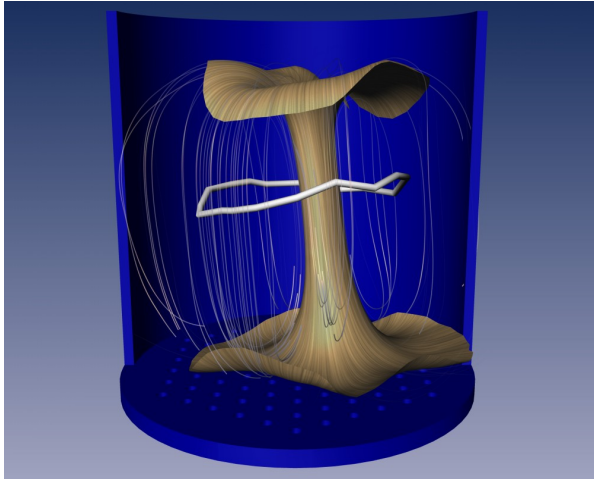
We propose the following measures to be used for an iconic representation of Galilean invariant vortex core lines:

- *Strength/Value of vortex region quantity s* : Our vortex core lines are linked directly to a vortex region quantity s and their extremum property with respect to s ensures, that no regions indicating stronger vortex activity exist away from the extracted features. Furthermore, the value of s varies along a line. To distinguish between (parts of) core lines with different vortical activity, the value of s should be encoded in the line representation. We found coloring and scaling most suitable for this.
- *Sign of rotation angle φ* : As shown in section 2.1, the rotation angle φ is derived from the Jacobian of the vector field. Its sign gives the direction of rotation of a vortex. As a visual encoding for this, the usage of color, twist or an orbit seems to be most appropriate.
- *Strength of rotation Δ* : This measure indicates the strength of spiraling patterns in the right reference frame. We found the usage of color, twist or an orbit most suitable for this.

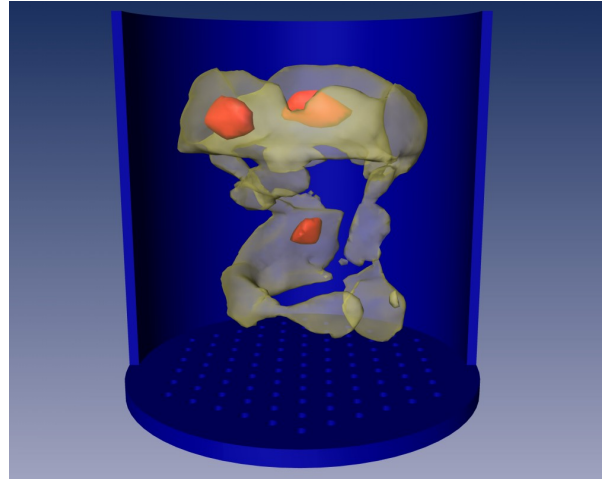
We apply these visualization strategies in different combinations in the next section.

5. Applications

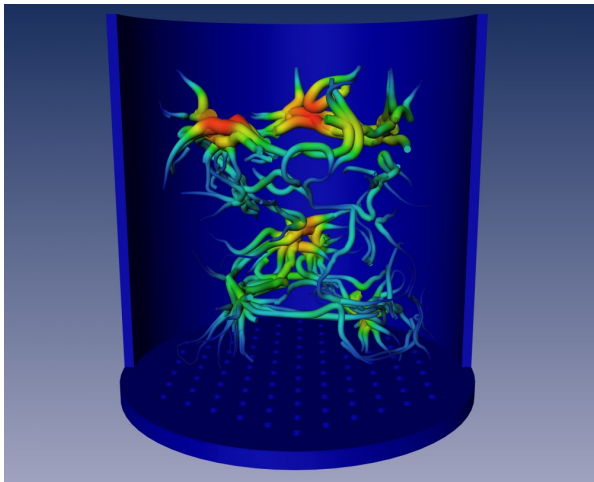
Figures 1 and 4 visualize a snapshot of a transitional wake behind a circular cylinder [ZFN*95]. This data set was derived from a direct numerical simulation of the Navier-Stokes equation by Bernd R. Noack (TU Berlin). It is given on a $88 \times 106 \times 20$ uniform grid. The data resolves the so-called ‘mode A’ of the 3D transition at a Reynolds number



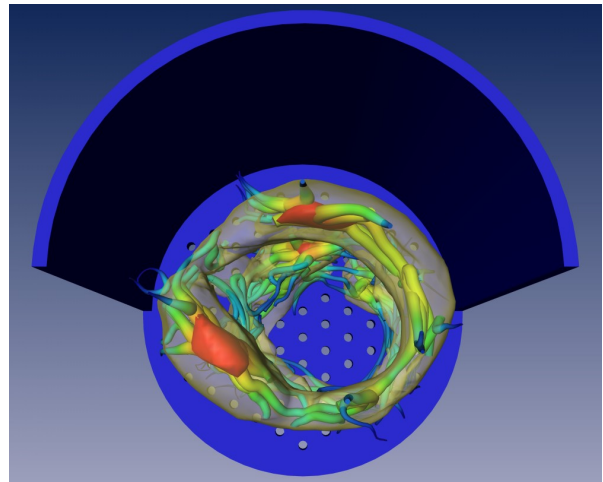
(a) Visualized using illuminated field lines [ZSH96] and a LIC-textured stream surface [BSH96]. Vortex core lines following the approach of [SH95, PR99] displayed as gray lines.



(b) Isosurfaces of λ_2 .



(c) Galilean invariant vortex core lines.



(d) Comparison between λ_2 -isosurfaces and our vortex core lines. View from top.

Figure 5: Bubble chamber. Vortex core lines extracted, colored and scaled according to λ_2 . Same colormap as in figure 4.

of 200 and at a spanwise wavelength of 4 diameters. This flow exhibits periodic vortex shedding leading to the well known von Kármán vortex street. This phenomenon plays an important role in many industrial applications, like mixing in heat exchangers or mass flow measurements with vortex counters. However, this vortex shedding can lead to undesirable periodic forces on obstacles, like chimneys, buildings, bridges and submarine towers. The chain of vortices with their alternating orientation of rotation is clearly depicted in figure 4 due to the usage of spiraling orbits. This is a major property of the von Kármán vortex street. Furthermore, it can be seen that downstream the vortices loose their strength.

Figure 5 shows the geometry of a bubble chamber and its interior flow. The flow has been measured experimentally on a $11 \times 11 \times 10$ uniform grid by a biplanar x-ray angiography in a biofluidmechanics laboratory. The bubble chamber is used as a biochemical reactor. Air injection into the liquid through holes in the floor plate is used to improve the reaction. The dataset was provided by Axel Seeger, Biofluidmechanics Lab, Charite Berlin. Figure 5a shows a Galilean variant vortex core line according to [SH95, PR99] around which the flow spirals. Figure 5b shows isosurfaces of λ_2 corresponding to different isovalues. In Figure 5c, the vortex core lines with respect to λ_2 extracted by our method are

shown, sized and coloured corresponding to λ_2 . Figure 5d is a combination of Figures 5b and 5c looking into the bubble chamber from above. This figure clearly shows that our approach yields vortex core lines in the center of the considered vortex region quantity.

Figure 6 shows the transitional flow around a backward-facing step. The flow field is obtained from a numerical simulation of Kaltenbach and Janke (both TU Berlin) at a Reynolds number of $Re_H=3000$ based on oncoming velocity and on step height. The corresponding boundary conditions are described in [KJ00]. The data set is given on a $266 \times 64 \times 128$ rectilinear grid. Figure 6a shows stream lines of the velocity field with respect to the original frame of reference. The vortex region quantity Q is visualized in figure 6b. This already gives an overview of the vortical structures inherent to this flow, but the visualization strongly depends on the choice of a transfer function. Figures 6c-d elucidate the dominant vortical structures by scaling and coloring the vortex core lines according to Q . This clearly shows that the depiction of Galilean invariant vortex core lines yields expressive visualizations even for very complex settings.

6. Conclusions

In this paper we made the following contributions:

- We proposed using ridge or valley lines of vortex region quantities to extract Galilean invariant vortex core lines.
- We proposed a generalization of this concept by giving a definition of d -dimensional Galilean invariant vortex cores.
- We discussed implementation issues for our method including how to choose an appropriate approximation scheme.
- We proposed an iconic representation of Galilean invariant vortex core lines.

A drawback of our method is that it requires second order derivatives. In order to investigate the dependence of our method to the chosen interpolation or approximation scheme, we plan to test further schemes and to compare the results.

For the future we plan to extract higher dimensional vortex cores as defined in subsection 2.3. For this it might be necessary to consider other quantities than mentioned in this paper.

The application to a number of data sets shows the feasibility of our method even for complex settings. We conclude that the visualization of Galilean invariant vortex core lines supports the interpretation of both strength and extent of vortical flow structures.

Acknowledgment

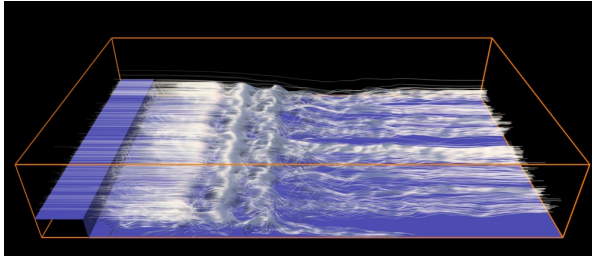
We thank Holger Theisel for the constant collaboration. We thank Bernd R. Noack for the fruitful discussions and the

supply of the cylinder data set. We acknowledge the support of Kaltenbach and Janke regarding the step data set. We thank Axel Seeger and Klaus Affold for the supply of the bubble chamber data set.

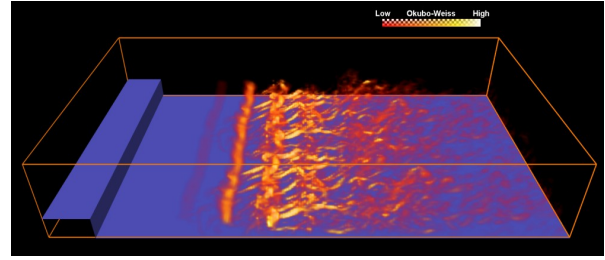
All visualizations in this paper have been created using AMIRA – a system for advanced visual data analysis [SWH05] (see <http://amira.zib.de/>).

References

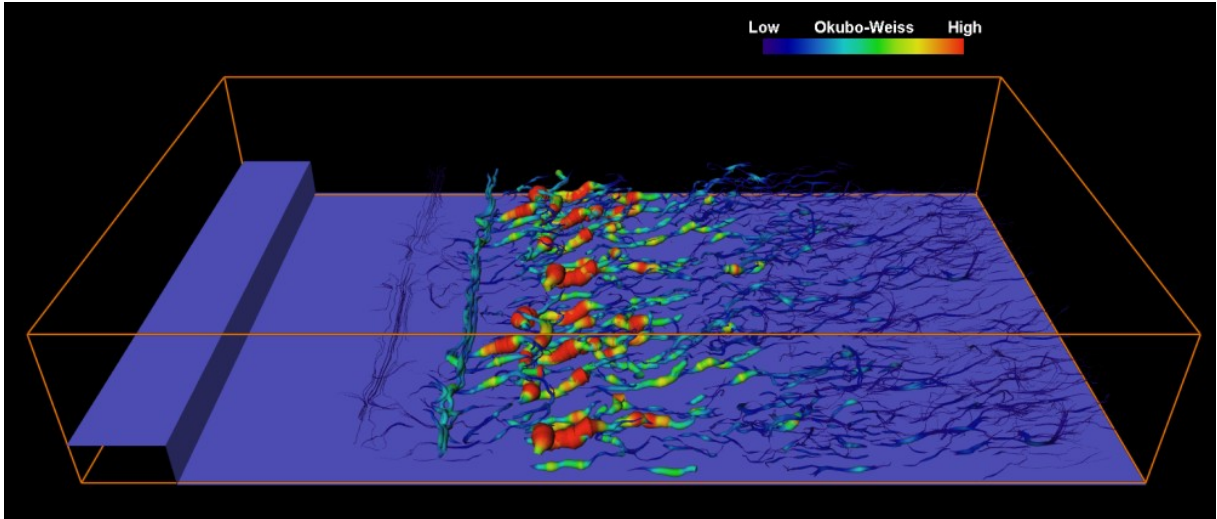
- [BS95] BANKS D., SINGER B.: A predictor-corrector technique for visualizing unsteady flow. *IEEE Transactions on Visualization and Computer Graphics* 1, 2 (1995), 151–163. 1, 3
- [BSH96] BATTKE H., STALLING D., HEGE H.-C.: *Visualization and Mathematics 1997*. Springer, Heidelberg, 1996, ch. Fast Line Integral Convolution for Arbitrary Surfaces in 3D, pp. 181–195. 7
- [CPC90] CHONG M. S., PERRY A. E., CANTWELL B. J.: A general classification of three-dimensional flow fields. *Physics of Fluids A* 2, 5 (1990), 765–777. 2
- [dLvL99] DE LEEUW W., VAN LIERE R.: Collapsing flow topology using area metrics. In *Proc. IEEE Visualization '99* (1999), pp. 149–354. 1
- [Ebe96] EBERLY D.: *Ridges in Image and Data Analysis*. Kluwer Academic Publishers, Dordrecht, 1996. 3, 4, 5
- [EGM*94] EBERLY D., GARDNER R., MORSE B., PIZER S., SCHARLACH C.: Ridges for image analysis. *Journal of Mathematical Imaging and Vision* 4, 4 (1994), 353–373. 3
- [GLL91] GLOBUS A., LEVIT C., LASINSKI T.: A tool for visualizing the topology of three-dimensional vector fields. In *Proc. IEEE Visualization '91* (1991), pp. 33–40. 1
- [GTS04] GARTH C., TRICOCHÉ X., SCHEUERMANN G.: Tracking of vector field singularities in unstructured 3D time-dependent datasets. In *Proc. IEEE Visualization 2004* (2004), pp. 329–336. 1
- [HH89] HELMAN J., HESSELINK L.: Representation and display of vector field topology in fluid flow data sets. *IEEE Computer* 22, 8 (August 1989), 27–36. 1
- [Hun87] HUNT J.: Vorticity and vortex dynamics in complex turbulent flows. *Proc CANCAM, Trans. Can. Soc. Mec. Engrs* 11 (1987), 21. 3
- [JH95] JEONG J., HUSSAIN F.: On the identification of a vortex. *J. Fluid Mechanics* 285 (1995), 69–94. 1, 3
- [JMT02] JIANG M., MACHIRAJU R., THOMPSON D.: Geometric verification of swirling features in flow fields. In *Proc. IEEE Visualization 2002* (2002), pp. 307–314. 6
- [KJ00] KALTENBACH H.-J., JANKE G.: Direct numerical simulation of flow separation behind a swept, rearward-facing step at $re_H=3000$. *Physics of Fluids* 12 (2000), 2320–2337. 8



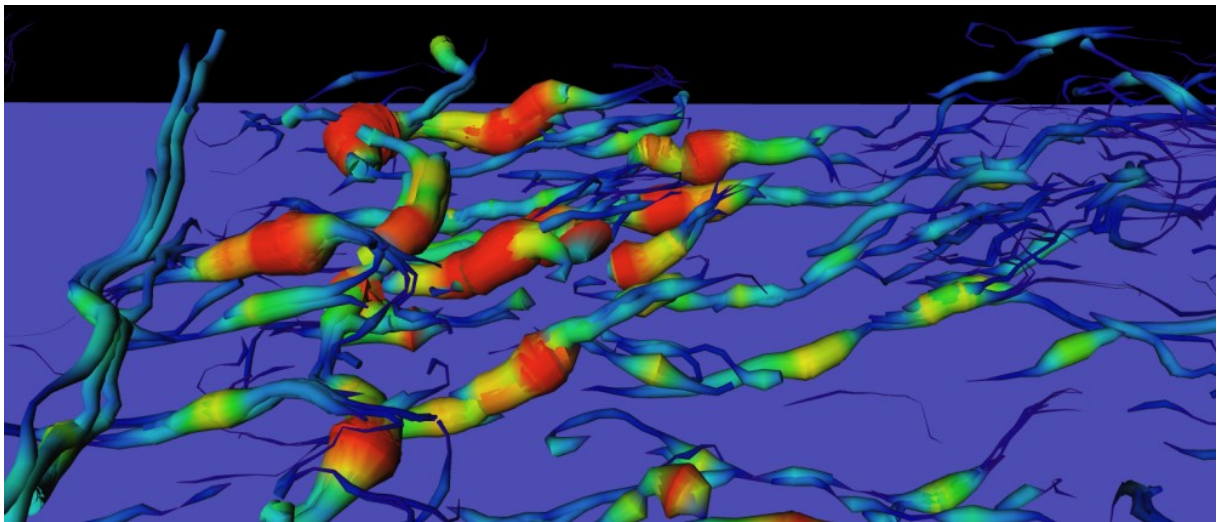
(a) Visualized using illuminated field lines with curvature-based seeding [WT02, WHN*03].



(b) Volume rendering of Q .



(c) Galilean invariant vortex core lines.



(d) Close up.

Figure 6: Flow around a backward-facing step. Vortex core lines extracted, colored and scaled according to Q .

- [KvD93] KOENDERINCK J. J., VAN DOORN A.: Local features of smooth shape: Ridges and courses. *SPIE Proc. Geometric Methods in Computer Vision II*, 2031 (1993), 2–13. [3](#)
- [MK97] MIURA H., KIDA S.: Identification of tubular vortices in turbulence. *Journal of the Physical Society of Japan* 66, 5 (1997), 1331–1334. [3](#)
- [PFTV91] PRESS W., FLANNERY B., TEUKOLSKY S., VETTERLING W.: *Numerical Recipes in C: The Art of Scientific Computing*. Cambridge University Press, Cambridge, 1991. [5](#)
- [Pow64] POWELL M. J. D.: An efficient method for finding the minimum of a function of several variables without calculating derivatives. *The Computer Journal*, 7 (1964), 155–162. [5](#)
- [PR99] PEIKERT R., ROTH M.: The parallel vectors operator - a vector field visualization primitive. In *Proc. Visualization 99* (1999), pp. 263–270. [1](#), [2](#), [3](#), [4](#), [5](#), [7](#)
- [PVH*02] POST F., VROLIJK B., HAUSER H., LARAMEE R., DOLEISCH H.: Feature extraction and visualisation of flow fields. In *Proc. Eurographics 2002, State of the Art Reports* (2002), pp. 69–100. [1](#)
- [RP96] ROTH M., PEIKERT R.: Flow visualization for turbomachinery design. In *Proc. Visualization 96* (1996), pp. 381–384. [1](#), [3](#)
- [RP98] ROTH M., PEIKERT R.: A higher-order method for finding vortex core lines. In *Proc. IEEE Visualization '98* (Los Alamitos, 1998), Ebert D., Hagen H., Rushmeier H., (Eds.), IEEE Computer Society Press, pp. 143–150. [1](#), [3](#)
- [RZNS04] ROESSL C., ZEILFELDER F., NUERNBERGER G., SEIDEL H.-P.: Reconstruction of volume data with quadratic super splines. *IEEE Trans. Visualization and Computer Graphics* 10 (2004), 397–409. [5](#)
- [SH95] SUJUDI D., HAIMES R.: *Identification of swirling flow in 3d vector fields*. Tech. rep., Department of Aeronautics and Astronautics, MIT, 1995. AIAA Paper 95-1715. [1](#), [2](#), [3](#), [7](#)
- [SKMR98] SCHEUERMANN G., KRÜGER H., MENZEL M., ROCKWOOD A.: Visualizing non-linear vector field topology. *IEEE Transactions on Visualization and Computer Graphics* 4, 2 (1998), 109–116. [1](#)
- [SP03] SATO M., PEIKERT R.: Core-line-based vortex hulls in turbomachinery flows. *Journal of the Visualization Society of Japan* 23, 2 (2003), 151–154. [2](#), [4](#), [6](#)
- [SWH05] STALLING D., WESTERHOFF M., HEGE H.-C.: Amira: A highly interactive system for visual data analysis. *The Visualization Handbook* (2005), 749–767. [8](#)
- [TGK*04] TRICOCHÉ X., GARTH C., KINDLMANN G., DEINES E., SCHEUERMANN G., RUETTEN M., HANSEN C.: Visualization of intricate flow structures for vortex breakdown analysis. In *Proc. IEEE Visualization 2004* (2004), pp. 187–194. [1](#)
- [TS03] THEISEL H., SEIDEL H.-P.: Feature flow fields. In *Data Visualization 2003. Proc. VisSym 03* (2003), pp. 141–148. [3](#), [4](#)
- [TWH03] THEISEL H., WEINKAUF T., HEGE H.-C., SEIDEL H.-P.: Saddle connectors - an approach to visualizing the topological skeleton of complex 3D vector fields. In *Proc. IEEE Visualization 2003* (2003), pp. 225–232. [1](#)
- [WHN*03] WEINKAUF T., HEGE H.-C., NOACK B., SCHLEGEL M., DILLMANN A.: Coherent structures in a transitional flow around a backward-facing step. *Physics of Fluids* 15, 9 (September 2003), S3. Winning Entry from the Gallery of Fluid Motion 2003. [9](#)
- [WS01] WISCHGOLL T., SCHEUERMANN G.: Detection and visualization of closed streamlines in planar flows. *IEEE Transactions on Visualization and Computer Graphics* 7, 2 (2001), 165–172. [1](#)
- [WT02] WEINKAUF T., THEISEL H.: Curvature measures of 3D vector fields and their applications. In *Journal of WSCG* (2002), vol. 10:2, pp. 507–514. [9](#)
- [WTH04] WEINKAUF T., THEISEL H., HEGE H.-C., SEIDEL H.-P.: Topological construction and visualization of higher order 3D vector fields. *Computer Graphics Forum (Eurographics 2004)* 23, 3 (2004), 469–478. [1](#)
- [ZFN*95] ZHANG H.-Q., FEY U., NOACK B., KÖNIG M., ECKELMANN H.: On the transition of the cylinder wake. *Phys. Fluids* 7, 4 (1995), 779–795. [6](#)
- [ZSH96] ZÖCKLER M., STALLING D., HEGE H.: Interactive visualization of 3D-vector fields using illuminated stream lines. In *Proc. IEEE Visualization '96* (1996), pp. 107–113. [7](#)